Journal of Electrical Engineering & Technology
https://doi.org/10.1007/s42835-021-00796-4

ORIGINAL ARTICLE

Rooted Tree Optimization Algorithm to Improve DTC Response of DFIM

Youcef Bekakra[1] · Yacine Labbi[1] · Djilani Ben Attous[1] · Om P. Malik[2]

Received: 10 February 2020 / Revised: 6 September 2020 / Accepted: 20 May 2021

Abstract
In this paper, an integral-proportional (IP) controller is employed in speed loop control in direct torque control (DTC) of a doubly fed induction motor (DFIM). Using IP parameters obtained from classical tuning methods, such as pole placement method, Ziegler–Nichols, etc., has disadvantages like high undershoot and overshoot, slow settling time, etc. To overcome the drawbacks of the classical methods, a new approach in which the IP controller parameters are tuned by rooted tree optimization (RTO) algorithm minimizing a multi-objective function is presented. The proposed algorithm has been verified and tested in control system with a PID controller. It presents improvement in performance response of various processes of different order compared with techniques such as Ziegler–Nichols, Kitamori's, Fuzzy-PID and Iterative Feedback Tuning. In addition, simulation results of direct torque control response of a DFIM with an IP controller designed using the RTO algorithm minimizing a multi-objective function show its effectiveness and better performance in speed response. Robustness test against parameter sensitivity for the proposed DTC-DFIM-RTO is verified under stator resistance variation.

Keywords Doubly fed induction machine · Direct torque control · Pole placement method · Ziegler–Nichols method · Rooted tree optimization

1 Introduction

The doubly fed induction machine has advantages compared to the conventional squirrel cage induction machine. It can be fed and controlled through its stator or rotor by diverse possible combinations and has been proposed in the literature [1, 2], among other industrial applications, as motor in high power applications such as traction, propulsion, etc., and as generator in wind energy conversion systems and pumped storage systems, etc. [3, 4].

✉ Youcef Bekakra
youcef-bekakra@univ-eloued.dz

Yacine Labbi
yacine-labbi@univ-eloued.dz

Djilani Ben Attous
dbenattous@yahoo.com

Om P. Malik
maliko@ucalgary.ca

[1] LEVRES Laboratory, University of El Oued, 39000 El Oued, Algeria

[2] Department of Electrical and Computer Engineering, University of Calgary, Calgary, AB, Canada

Among the various methods used to control the DFIM, the field oriented control (FOC) or vector control (VC) allows a decoupling between the torque and flux to obtain an independent control of torque and flux like a separately excited DC motor [3]. Decoupling the control scheme requires compensation for the coupling effect between d- and q-axes currents dynamics [5]. It is well known that VC needs quite complicated coordinate transforms to decouple the interaction between torque control and flux control to provide fast torque control on-line. In recent years another control method, called direct torque control, has gained the interest of researchers.

Direct torque control (DTC) provides better steady-state and transient torque control performance compared to the FOC techniques [6]. In addition, DTC does not require current regulators, nor coordinate transformations or specific modulations like Pulse Width Modulation (PWM) for pulse generation [7–14].

Ziegler–Nichols [15], Kitamori's [16], Fuzzy-PID [17], Iterative Feedback Tuning (IFT) [18]… etc., methods are used to tune proportional, integral and derivative (PID) controller parameters, but it is often difficult to find optimal gains with these approaches. Many other optimization

Published online: 02 June 2021

methods based on metaheuristic techniques, such as genetic algorithm [19], particle swarm optimization [20], have shown effectiveness to tune the PID controller parameters [21, 22], and are presented in many published scientific papers [23–31].

In [7], a new combined direct torque control with genetic algorithm (DTC-GA) based PI controller is applied to improve the classical DTC of a doubly fed induction machine. Improvements of this combined method are related to performance in torque and flux ripples, overshoot and response time. Adaptive fuzzy logic controllers and particle swarm optimization are proposed in [20] to improve DTC performance by adjusting the PI parameters where the results show better dynamic and steady-state performance. A new optimization method, named rooted tree optimization (RTO), proposed in [32] is applied to the economic dispatch problem and validated on a set of standard benchmark nonlinear functions.

In [33], hybrid technique based on fuzzy logic and RTO is presented for the strategic integration of distributed generation (DG) and distributed static compensator (DSTATCOM) in radial distribution system for improving profile of voltage, reducing losses, and maximizing economic and environmental benefits. The authors in [34] have proposed an optimized protection coordination with RTO algorithm in order to best solve the overcurrent relays problem. Simulation results show that the RTO with certain parameter settings operates better compared to the other algorithms. DSTATCOM and wind turbine type DG in distribution network (DN) based on RTO algorithm, is presented in [35], to enhance the voltage profile, maximize economic benefit, reduce loss, and decrease pollution level. In this work, the proposed strategy is examined on 33-bus DN. Obtained results confirm the effectiveness of the proposed compared with other algorithms.

RTO is used in [36] to adjust the parameters (K_p and K_i) of PI controller in order to reduce the chattering phenomena in active and reactive powers of doubly fed induction generator (DFIG), and to minimize the harmonic currents which appear frequently at the level of the rotor side converter in a doubly fed induction generator. In [37], RTO is employed to optimize high order sliding mode control based on the super-twisting approach to reduce torque and flux ripples for control of DFIG based on direct torque control scheme.

In multi-objective optimization problems, it is desirable to use multi-objective optimization algorithms [38]. The goal of multi-objective optimization problems (problems with more than one minimization goal) is to find the best compromise between multiple and conflicting objectives. However, it is usually difficult to find an optimal solution that satisfies conflicting objectives as there is not a single best solution being better than the others with respect to each objective.

The advantage of PID controller is its feasibility and ease of implementation. However, design of the conventional PID gains is not an easy task with in the presence of uncertainty. In this case, the controller requires tuning for obtaining better performance. Many methods are reported in the literature to do this, such as fuzzy logic [39], neural networks [40] and other methods like optimization techniques which can be used to find optimal controller gains in order to improve the performance of the system to be controlled. Among them, RTO algorithm which is proposed and applied in this paper for both controllers PID and IP. RTO is a recently technique, it based on the behavior of tree roots of a plant searching for the nearest location of water (best solution).

In this paper, PID controller based on the proposed RTO algorithm is investigated and tested in control system for various linear processes of different order. On the other hand, IP controller based RTO algorithm is examined in DTC technique for the DFIM. Mathematical model of this machine is inherently nonlinear, thus, make the control of DFIM difficult and calls for use of a high performance control approach like FOC and DTC. DTC strategy is applied to DFIM in order to directly control the flux and torque. RTO algorithm is proposed for tuning and obtaining optimal gains for both controllers PID and IP in order to overcome the drawbacks of the conventional tuning methods and obtain better performance.

In this paper, DFIM is controlled using DTC strategy. The speed is regulated by using an IP controller. In order to improve the performance of DTC-DFIM response like to minimize the settling time, reduce the undershoot and overshoot under load disturbance variation, RTO algorithm is proposed to tune IP controller gains (K_i and K_p) and compared to the conventional method (pole placement). Simulation results show that the proposed approach gives better performance (most reduced values of all indices in terms of integral square error (ISE) and integral absolute error (IAE)) than the other cases of the conventional method.

As a summary, the main contribution of this paper according to the PID controller and DFIM performance, compared to the conventional methods, is summarized as below:

- RTO algorithm presents another mechanism based on the movement of plant roots while looking for the nearest place of water (i.e., a solution).
- Simplicity of the implementation of this algorithm.
- RTO algorithm is applied to a new optimization problem in control system (PID controller) to find the optimum gains K_p, K_i and K_d because it is difficult to find their optimum values with classical tuning methods.

- RTO algorithm is applied to optimize an IP speed controller used in DTC-DFIM which shows a fast speed response (a smaller settling time) with more stability (a reduced overshoot) in transient state.
- Maximum undershoot and overshoot of the speed response of DFIM are reduced with the proposed DTC-RTO in transient and steady state.
- The proposed approach gives better performance in terms of ISE and IAE of the speed response of DFIM than the conventional method, therefore, a small area of error between the command and the output of the speed.

This paper is organized as follows: the DFIM model is presented in Sect. 2 and DTC of the DFIM is presented in Sect. 3. RTO concept and its mathematical equations are presented in Sect. 4. Application of RTO minimizing a multi-objective function applied to a PID controller is explained in Sect. 5. Tuning of the IP controller using two methods is described in Sect. 6. Simulation results are discussed in Sect. 7 and the conclusions are drawn in Sect. 8.

2 DFIM Model

The general electrical state model of the induction machine in $\alpha\beta$-coordinates is given by the following equations [41, 42]:

Stator and rotor voltages:

$$\begin{cases} V_{s\alpha} = R_s.i_{s\alpha} + \frac{d}{dt}\varphi_{s\alpha} \\ V_{s\beta} = R_s.i_{s\beta} + \frac{d}{dt}\varphi_{s\beta} \\ V_{r\alpha} = R_r.i_{r\alpha} + \frac{d}{dt}\varphi_{r\alpha} + \omega.\varphi_{r\beta} \\ V_{r\beta} = R_r.i_{r\beta} + \frac{d}{dt}\varphi_{r\beta} - \omega.\varphi_{r\alpha} \end{cases} \quad (1)$$

Stator and rotor fluxes:

$$\begin{cases} \varphi_{s\alpha} = L_s.i_{s\alpha} + M.i_{r\alpha} \\ \varphi_{s\beta} = L_s.i_{s\beta} + M.i_{r\beta} \\ \varphi_{r\alpha} = L_r.i_{r\alpha} + M.i_{s\alpha} \\ \varphi_{r\beta} = L_r.i_{r\beta} + M.i_{s\beta} \end{cases} \quad (2)$$

Electromagnetic torque:

$$T_e = p(\phi_{s\alpha}.i_{s\beta} - \phi_{s\beta}.i_{s\alpha}) \quad (3)$$

Mechanical equation:

$$T_e - T_L = J.\frac{d\Omega}{dt} + f.\Omega \quad (4)$$

The state variable vector is: $X = \left[i_{s\alpha} i_{s\beta} i_{r\alpha} i_{r\beta}\right]^T$.
The state model can be written as:

$$\dot{X} = A.X + B.U \quad (5)$$

where A is an n-by-n matrix, n is the number of states, B is an n-by-m matrix, m is the number of inputs.

with:

$$\dot{X} = \left[\frac{d}{dt}i_{s\alpha}\frac{d}{dt}i_{s\beta}\frac{d}{dt}i_{r\alpha}\frac{d}{dt}i_{r\beta}\right]^T$$

$$U = \left[V_{s\alpha} V_{s\beta} V_{r\alpha} V_{r\beta}\right]^T$$

$$A = \begin{bmatrix} -a_1 & a.\omega & a_3 & a_5\omega \\ -a.\omega & -a_1 & -a_5\omega & a_3 \\ a_4 & -a_6\omega & -a_2 & -\frac{\omega}{\sigma} \\ a_6\omega & a_4 & \frac{\omega}{\sigma} & -a_2 \end{bmatrix},$$

$$B = \begin{bmatrix} b_1 & 0 & -b_3 & 0 \\ 0 & b_1 & 0 & -b_3 \\ -b_3 & 0 & b_2 & 0 \\ 0 & -b_3 & 0 & b_2 \end{bmatrix}.\text{where } a = \frac{1-\sigma}{\sigma},\ a_1 = \frac{R_s}{\sigma L_s},$$

$a_2 = \frac{R_r}{\sigma L_r}, a_3 = \frac{R_r M}{\sigma L_s L_r}, a_4 = \frac{R_s M}{\sigma L_s L_r}, a_5 = \frac{M}{\sigma L_s}, a_6 = \frac{M}{\sigma L_r}, b_1 = \frac{1}{\sigma L_s},$
$b_2 = \frac{1}{\sigma L_r}, b_3 = \frac{M}{\sigma L_s L_r}, \sigma = 1 - \frac{M^2}{L_s L_r}.$

All symbols are defined in the Appendix Nomenclature.

3 Direct Torque Control

Direct Torque control was introduced in 1986 especially for the asynchronous machine [6, 43] and later for the synchronous one [44, 45]. The main advantages of DTC are:

- Simple control scheme without using current loops or a pulse width modulation (PWM) modulator.
- The control does not require coordinate transformation between the stationary frame and the synchronous frame.
- Has low sensitivity to parameter variations.
- It is possible to obtain good dynamic control of torque without any mechanical transducers on the machine shaft.
- Has fast torque dynamic response.

The basic configuration of DTC applied to a DFIM is presented in Fig. 1. The flux and torque are controlled directly and independently by the selection of optimum inverter voltage vectors to limit their errors. Outputs of the three level torque hysteresis comparator, two level flux hysteresis comparator and stator flux position are used to obtain the optimum stator voltage vector through a switching table [46].

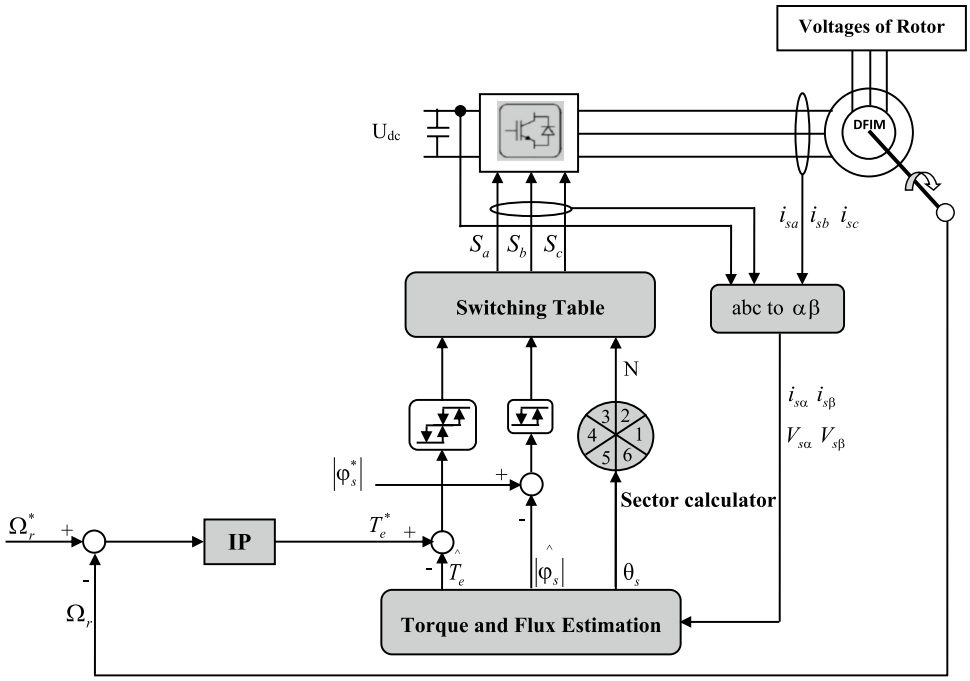

Fig. 1 DTC diagram of DFIM with an IP controller

3.1 Stator Flux and Electromagnetic Torque Estimation

Magnitude of stator flux can be estimated by [19]:

$$\left|\hat{\phi}_s\right| = \sqrt{\phi_{s\alpha}^2 + \phi_{s\beta}^2} \tag{6}$$

where:

$$\phi_{s\alpha} = \int_0^t (V_{s\alpha} - R_s i_{s\alpha})dt \tag{7}$$

$$\phi_{s\beta} = \int_0^t (V_{s\beta} - R_s i_{s\beta})dt \tag{8}$$

Angle of the stator flux can be given by:

$$\theta_s = arctg\frac{\phi_{s\beta}}{\phi_{s\alpha}} \tag{9}$$

Electromagnetic torque can be estimated by stator flux and stator currents as given by Eq. (3).

3.2 Switching Table

A typical space vector diagram of a two-level inverter is shown in Fig. 2.

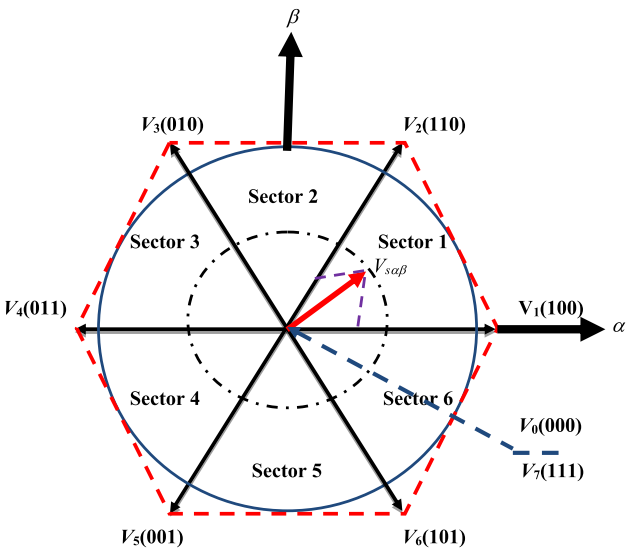

Fig. 2 Diagram of voltage space vector

The possible global locus is divided into six different sectors as signaled by the discontinuous line. Accordingly, a six sector switching table [7, 47] is derived as given in Table 1.

Direct torque control is based on the stator flux orientation, using the instantaneous values of the voltage vector. Among the eight voltage vectors provided by the inverter, two vectors are zeros [48]. These vectors are chosen from a switching table according to the flux and torque errors as

well as the stator flux vector position. The eight voltage vectors which correspond to possible inverter states are shown in Table 2.

4 Rooted Tree Optimization

The roots of tree start to search for water from the top of the stalk which in turn spreads its roots in the first layer of soil (initial generation), these roots go to search for water in a random way where the root that is the nearest to the degree of wetness will become the knot from which the new generation of roots begins search again for the best place (best solution) to get water [37].

The Rooted Tree Optimization (RTO) algorithm is a relatively new algorithm proposed in 2016 [32]. It simulates the behavior of roots of desert plants searching for water as shown in Fig. 3.

4.1 Equations of RTO

Like other methods, the rooted tree optimization algorithm starts by creating an initial random population. In RTO algorithm, one "*root*" represents a suggested solution and a "*Wetness Degree* (D_w)" represents the evaluation of a candidate giving its fitness degree among the remaining population.

Table 1 Switching table for DTC

Flux	Torque	Sector					
$d\varphi_s$	dT_e	S_1	S_2	S_3	S_4	S_5	S_6
1	1	V_2	V_3	V_4	V_5	V_6	V_1
	0	V_0	V_7	V_0	V_7	V_0	V_7
	-1	V_6	V_1	V_2	V_3	V_4	V_5
0	1	V_3	V_4	V_5	V_6	V_1	V_2
	0	V_7	V_0	V_7	V_0	V_7	V_0
	-1	V_5	V_6	V_1	V_2	V_3	V_4

Table 2 Switch positions and their voltage vectors

	V_0	V_1	V_2	V_3	V_4	V_5	V_6	V_7
S_a	0	1	1	0	0	0	1	1
S_b	0	0	1	1	1	0	0	1
S_c	0	0	0	0	1	1	1	1

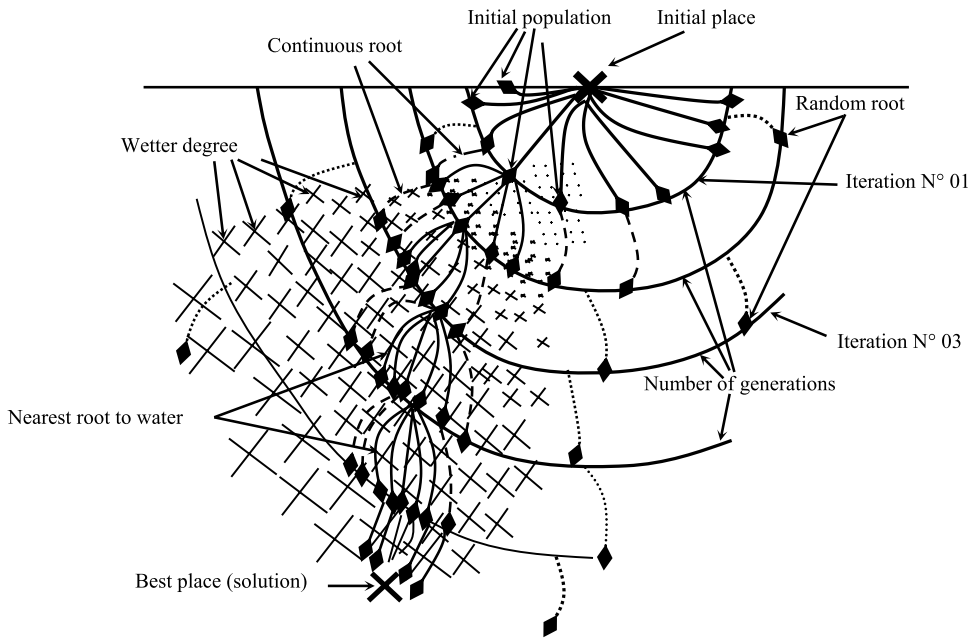

Fig. 3 Behavior of the roots of the desert plants searching for water

4.1.1 Rate of the Nearest Root to Water (R_n)

This rate represents the number of candidates according to the total population that should gather around the wetter place (the best solution). The new population of the nearest root to water is given by:

$$x^{new}(k,\ iter+1) = x^{best}(iter) + c_1 \times D_w(k) \times randn \times upper/(N \times iter) \tag{10}$$

where *iter*: iteration step, $x^{new}(k,\ iter+1)$: new candidate for the iteration $(iter+1)$, $x^{best}(iter)$: best solution from the previous generation, k: candidate number, N: population scale, *upper*: upper limit of the parameter, *randn*: normal random number between [− 1, 1].

4.1.2 Rate of the Continuous Root in Its Orientation (R_c)

It represents the rate of members who have continued/forwarded the previous way because they appear near the water. The new population of the random root is presented by:

$$x^{new}(k,\ iter+1) = x(k,\ iter) + c_2 \times D_w(k) \times rand \times (x^{best}(iter) - x(k,\ iter)) \tag{11}$$

where $x(k,\ iter)$: candidate for the previous iteration *iter*, *rand*: number between [0, 1].

4.1.3 Rate of the Random Root (R_r)

It represents the rate of the number of candidates according to the total population that they will spread randomly in the research space to increase the rate of getting the global solution. They also replace the roots with a weak wetness degree from the last generation. The new population of the random root is given by:

$$x^{new}(k, iter+1) = x_r(iter) + c_3 \times D_w(k) \times randn \times upper/iter \tag{12}$$

where: $x_r(iter)$: randomly selected individual from the previous generation, c_1, c_2 and c_3 are adjustable parameters.

The rates R_n, R_r and R_c are determined experimentally according to the problem under study. They are considered as variables which affect convergence [32].

4.2 RTO Algorithm

The steps of RTO algorithm can be listed as below:

Step 1

Create an initial generation, composed of N candidates, randomly within the variables limits in the research space and determine the numerical values of rates R_n, R_r and R_c.

Step 2

Evaluate all population members to calculate their objective function (wetness degree (D_w)) as:

$$D_w(k) = \begin{cases} \dfrac{f_k}{\max(f_k)} & \text{for the maximum objective function} \\ 1 - \dfrac{f_k}{\max(f_k)} & \text{for the minimum objective function} \end{cases}, \quad k = 1, 2, \ldots, N \tag{13}$$

Step 3

Reproduce and replace by the new population. Reorder the population according to the wetness degree (D_w) to replace them by the new population according to R_n, R_r and R_c using Eqs. (10), (11) and (12).

Step 4

Return to step 2 if the stopping criteria is not met.

5 RTO Applied to PID Controller

To illustrate the effectiveness of the proposed method in control system, closed loop responses of a number of simulated systems to a unit step in reference input are presented. For PID controller problem, three different processes with different order (second, third and fourth order) [17] are considered as below:

$$G_1(s) = \frac{e^{-0.5s}}{(s+1)^2} \tag{14}$$

$$G_2(s) = \frac{4.228}{(s+0.5)(s^2+1.64s+8.456)} \tag{15}$$

$$G_3(s) = \frac{27}{(s+1)(s+3)^3} \tag{16}$$

In addition, the proposed algorithm and IFT method have been tested on the following three simulated systems [18]:

$$G_4(s) = \frac{e^{-5s}}{20s+1} \tag{17}$$

$$G_5(s) = \frac{1}{(10s+1)^8} \tag{18}$$

$$G_6(s) = \frac{(1-5s)e^{-3s}}{(10s+1)(20s+1)} \tag{19}$$

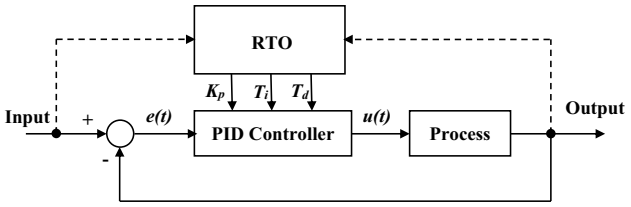

Fig. 4 Block diagram of a simplified control system based PID controller

Block diagram of a simplified control system is shown in Fig. 4.

In practice, output of the PID controller is given by:

$$u(t) = K_p\left[e(t) + \frac{1}{T_i}\int_0^t e(t)dt + T_d\frac{de(t)}{dt}\right] \tag{20}$$

Transfer function of the PID controller is:

$$G_{PID}(s) = K_p\left[1 + \frac{1}{T_i s} + T_d s\right] \tag{21}$$

where K_p is the proportional gain, T_i is the integral action time, T_d is the derivative action time and $e(t)$ is the error between the input and the output of the process at time 't'.

The goal of multi-objective optimization problems is to find the best compromise between multiple and clashing objectives. There will be more than one solution that optimizes at the same time all the objectives considered in these problems and there is no distinct superiority between these solutions. In general, there is not a single best solution being better than the other with respect to each objective.

In control system applications, the selected performance criterion is often a weighted combination of various performance characteristics such as settling time and overshoot. The desired system output should have a minimal settling time with a small or no overshoot in the step response of the closed loop system. Consequently, the objective function *Obj* is defined by the performance of the settling time (T_s) and the overshoot (O_{sh}) requirements.

The objective function must be set:

$$Obj = min\,(F) \tag{22}$$

where: $F = [f_1 f_2]^T$: vector of the objective functions, f_1: settling time (T_s), f_2: overshoot (O_{Sh}).

Consequently:

$$Obj = \alpha_1.f_1 + \alpha_2.f_2 \tag{23}$$

where α_1 and α_2 are adjustable parameters.

In Eq. (23), it is considered that the objective function is based only on the settling time and the overshoot because these two performances are, respectively, responsible for rapidity and stability of the system response. Fast settling time and small overshoot give a small area between input and output for a given process, consequently a small error in closed loop.

In this paper, PID controller will be examined with the proposed RTO to control various linear systems, $G_1(s)$, $G_4(s)$ and $G_6(s)$, with constant time delay. It is noted that in case of this time delay is variable with time, this controller may require frequent re-tuning to adapt its gains according to the variations of the system model to be controlled to ensure good stability and obtain better performance, because this controller has fixed gains obtained after an offline tuning based on the proposed RTO.

6 Tuning of the IP Speed Controller by Pole Placement Method and RTO

In speed control loop, an integral-proportional (IP) controller is used because it gives good response [49], especially at the rejection of the disturbance. In this section, an IP speed controller is tuned by two methods: the first is pole placement method (classical method) and the second is optimizing a multi-objective function, Eq. (23), using RTO.

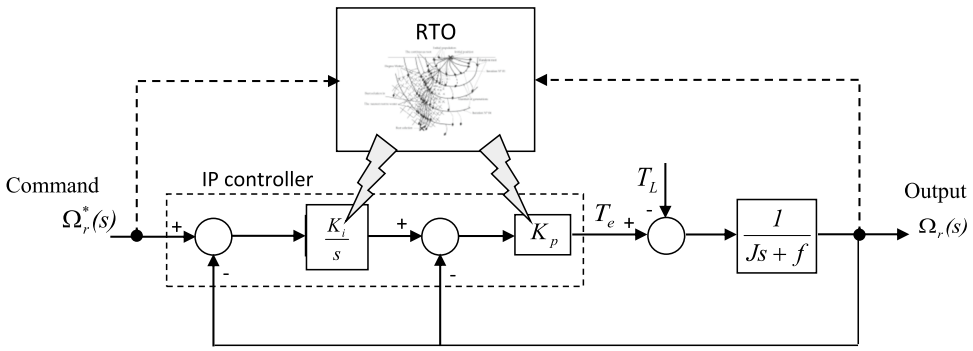

Fig. 5 IP speed controller tuned by RTO

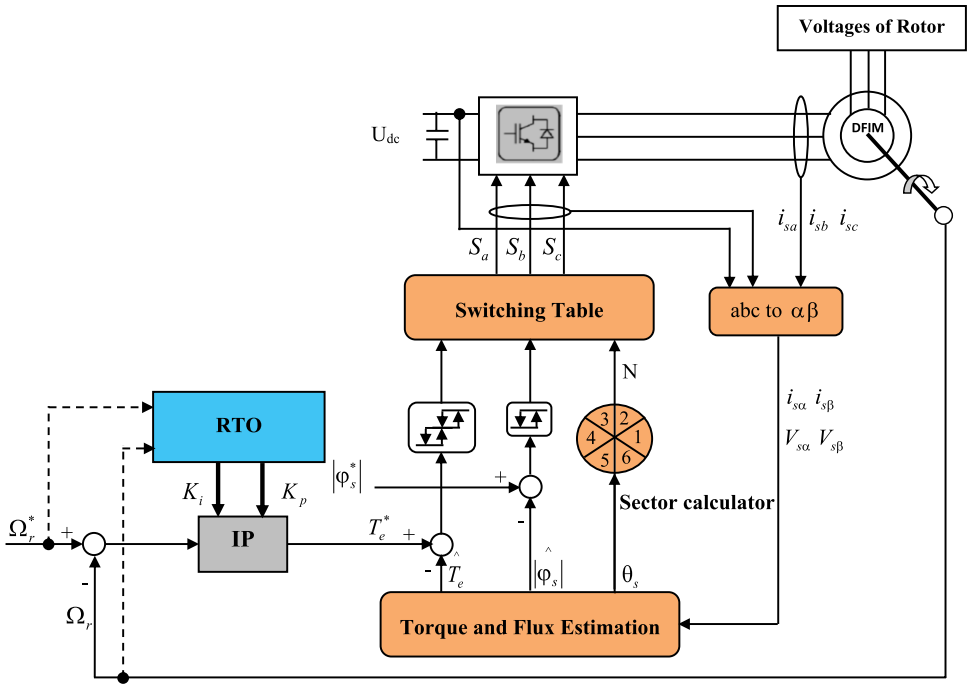

Fig. 6 DTC diagram of DFIM with IP controller tuned by RTO

To obtain optimum gains of the IP controller, K_i and K_p are generated by the RTO algorithm in each iteration based on command and output of the closed loop speed transfer function as shown in Fig. 5.

6.1 IP Speed Controller Tuned by Pole Placement Method

Based on Fig. 5, the closed loop speed transfer function is given by:

$$\frac{\Omega_r(s)}{\Omega_r^*(s)} = \frac{1}{\frac{J}{K_p K_i}s^2 + \frac{K_p+f}{K_p K_i}s + 1} \tag{24}$$

The closed loop transfer function in the form of a standard second-order system is given by:

$$F(s) = \frac{1}{\frac{1}{\omega_n^2}s^2 + \frac{2\xi}{\omega_n}s + 1} \tag{25}$$

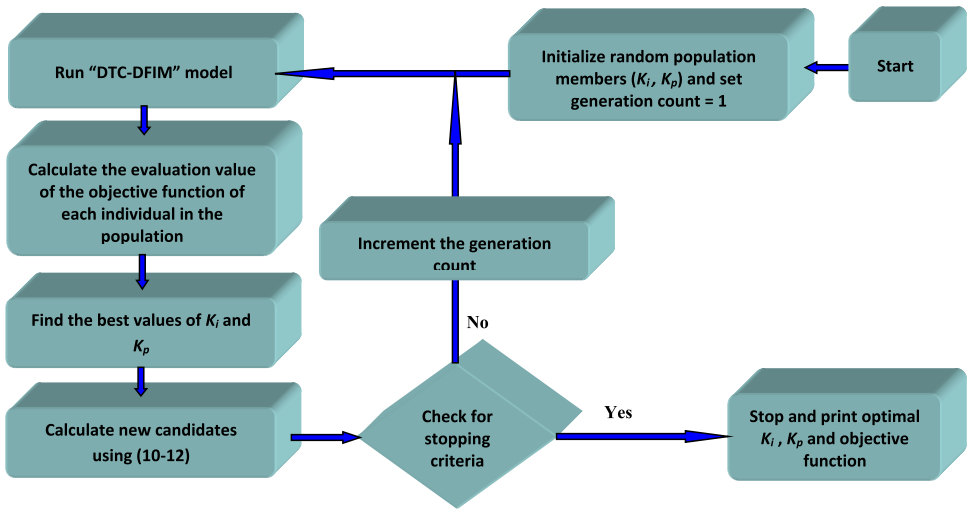

Fig. 7 Flow chart of RTO applied to IP controller in DTC of DFIM

Comparing Eqs. (24) and (25), obtains:

$$\begin{cases} \dfrac{J}{K_p K_i} = \dfrac{1}{\omega_n^2} \\ \dfrac{K_p + f}{K_p K_i} = \dfrac{2\xi}{\omega_n} \end{cases} \tag{26}$$

where

$$\begin{cases} K_p = 2J\xi\omega_n - f \\ K_i = \dfrac{J\omega_n^2}{K_p} = \dfrac{J\omega_n^2}{2J\xi\omega_n - f} \end{cases} \tag{27}$$

and K_p is proportional gain, K_i is integral gain, ξ is damping factor and ω_n is natural frequency.

Table 3 Parameters of RTO used in simulation

Parameter	Value
Population size	30
Maximum iteration	100
R_c	0.3
R_r	0.3
R_n	$1-(R_c+R_r)=0.4$
c_1	1.2
c_2	0.91
c_3	1.1

6.1.1 Stability Conditions of IP Speed Controller

Stability is required for good control system performance. Based on Eq. (24), which presents the closed loop speed transfer function with an IP controller, the denominator of this transfer function is given by:

$$D(s) = \frac{J}{K_p K_i}s^2 + \frac{K_p + f}{K_p K_i}s + 1 \tag{28}$$

The denominator roots ($D(s) = 0$) are the poles of the system described by Eq. (24). After calculations, they are obtained by:

$$\begin{cases} s_1 = -\frac{1}{2J}\left[K_p + f - \sqrt{(K_p)^2 + 2K_p f - 4JK_i K_p + f^2}\right] \\ s_2 = -\frac{1}{2J}\left[K_p + f + \sqrt{(K_p)^2 + 2K_p f - 4JK_i K_p + f^2}\right] \end{cases} \tag{29}$$

By replacing the values of the DFIM parameters, J and f (reported in Appendix 1), in Eq. (29), obtains:

$$\begin{cases} s_1 = -\frac{5}{2}\left[K_p - \sqrt{(K_p)^2 - \frac{4}{5}K_i K_p}\right] \\ s_2 = -\frac{5}{2}\left[K_p + \sqrt{(K_p)^2 - \frac{4}{5}K_i K_p}\right] \end{cases} \tag{30}$$

The system is said to be stable if all its poles lie in the left-half of the complex plane [50], in other word, all of its poles must have purely negative real parts.

We have:

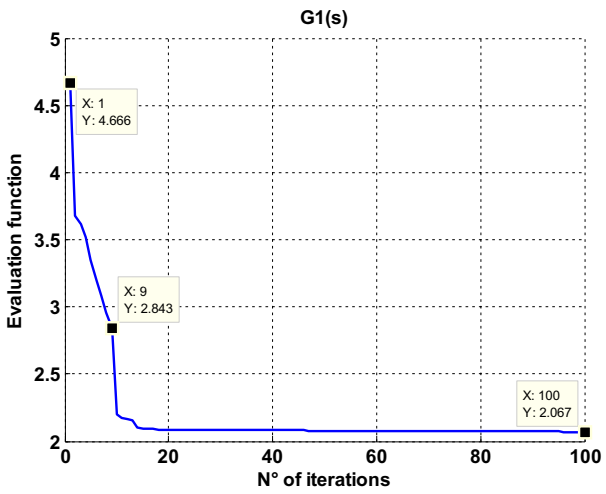

(a)

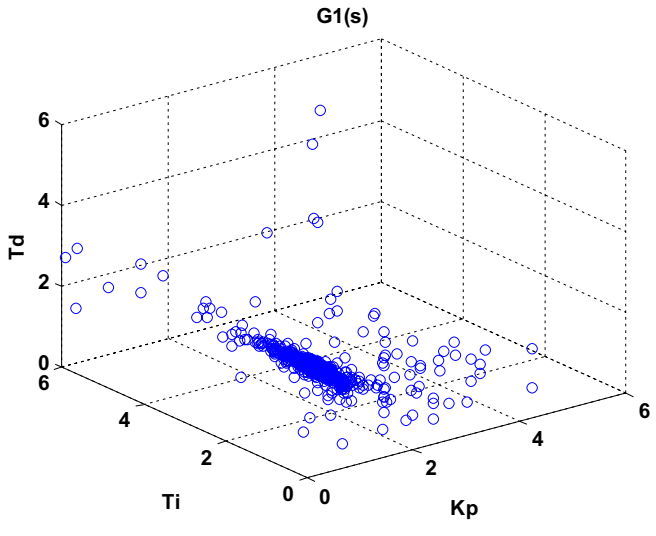

(b)

Fig. 8 **a** Evaluation function variation and **b** 3D concentration of the roots of "$G_1(s)$ process"

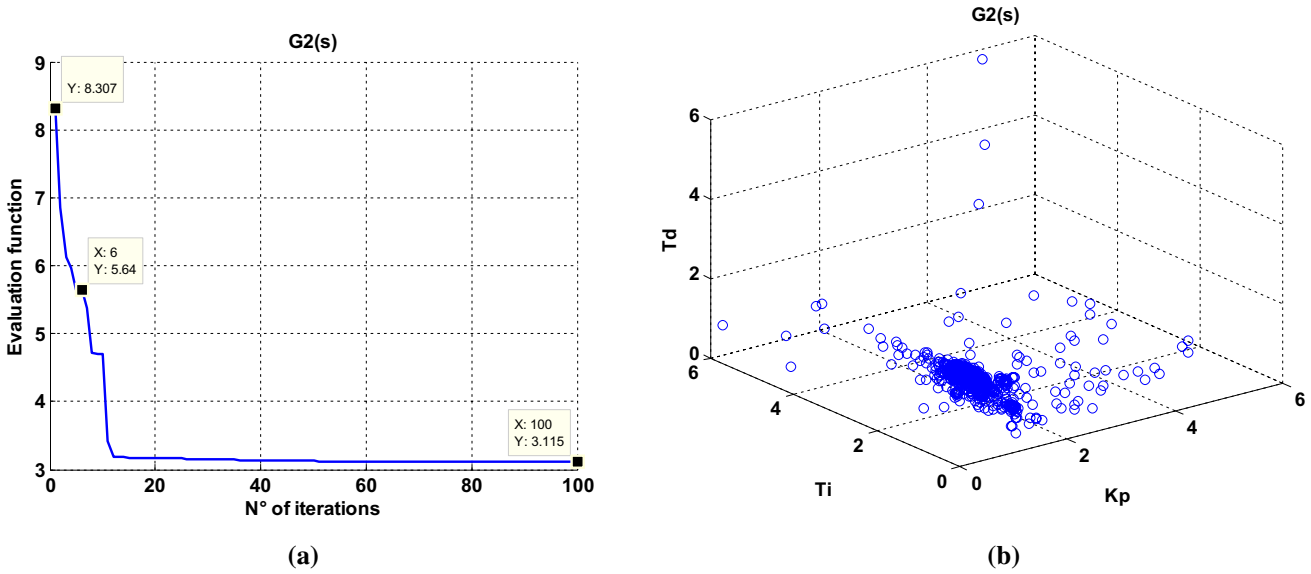

Fig. 9 **a** Evaluation function variation and **b** 3D concentration of the roots of "$G_2(s)$ process"

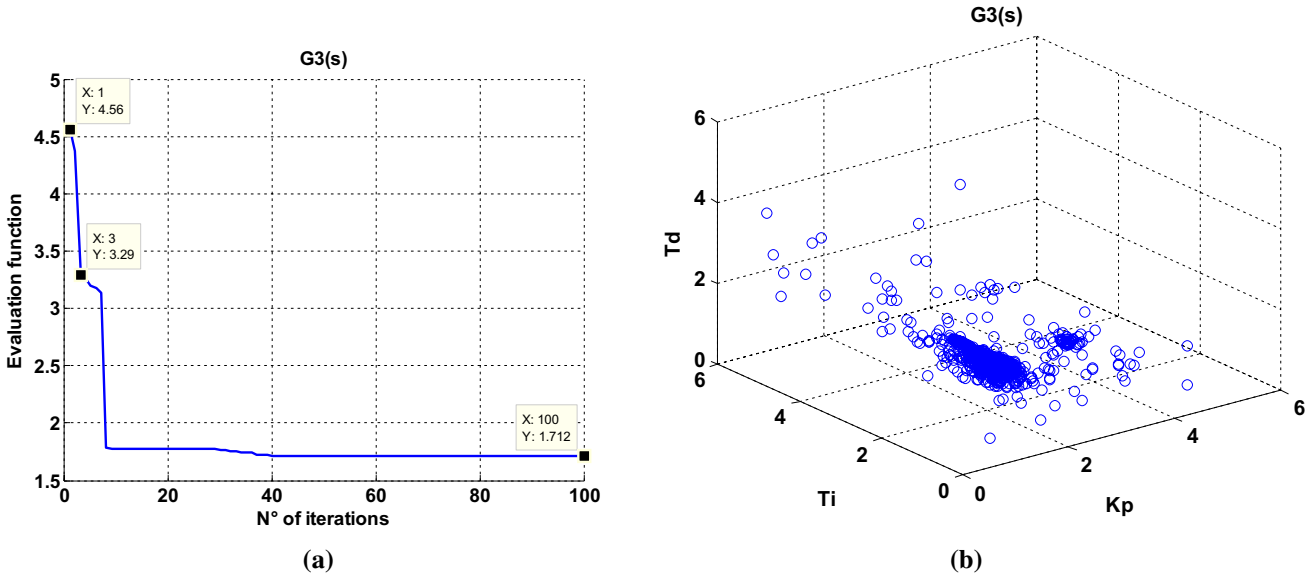

Fig. 10 **a** Evaluation function variation and **b** 3D concentration of the roots of "$G_3(s)$ process"

$$\begin{cases} s_1 = A_1 + jB_1 \\ s_2 = A_2 + jB_2 \end{cases} \tag{31}$$

where A_1 and A_2 are the real parts of the poles s_1 and s_2, respectively, B_1 and B_2 are the imaginary parts of the poles s_1 and s_2, respectively.

and,

$$\begin{cases} A_1 = -\frac{5}{2}\left[K_p - \sqrt{(K_p)^2 - \frac{4}{5}K_iK_p}\right] \\ B_1 = 0 \\ A_2 = -\frac{5}{2}\left[K_p + \sqrt{(K_p)^2 - \frac{4}{5}K_iK_p}\right] \\ B_2 = 0 \end{cases} \tag{32}$$

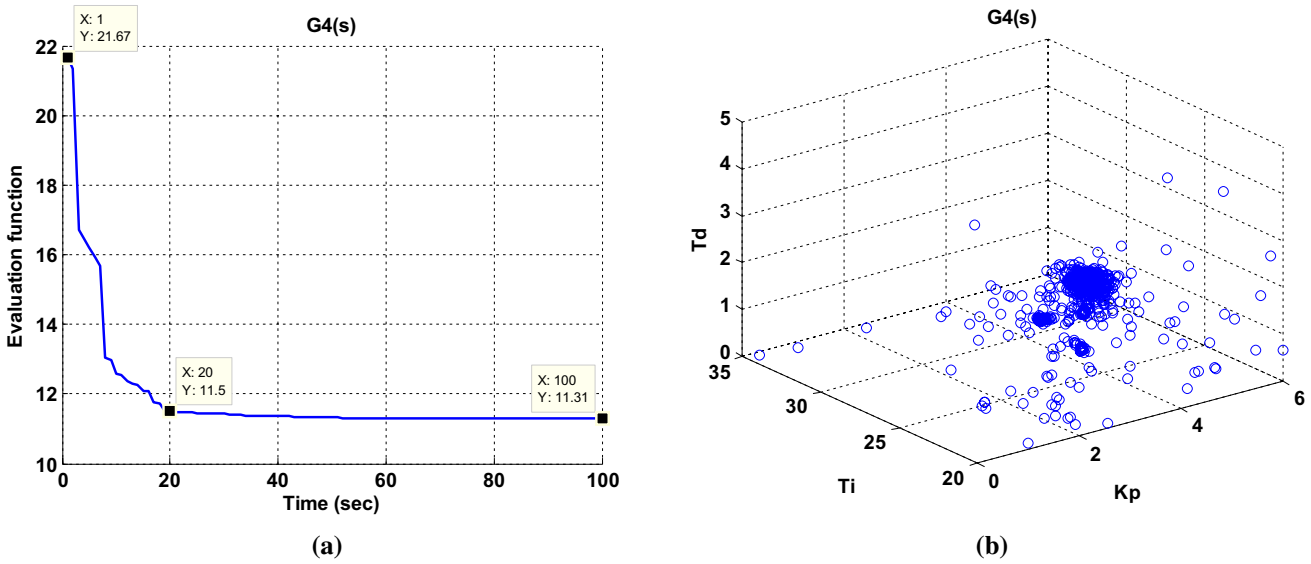

Fig. 11 **a** Evaluation function variation and **b** 3D concentration of the roots of "$G_4(s)$ process"

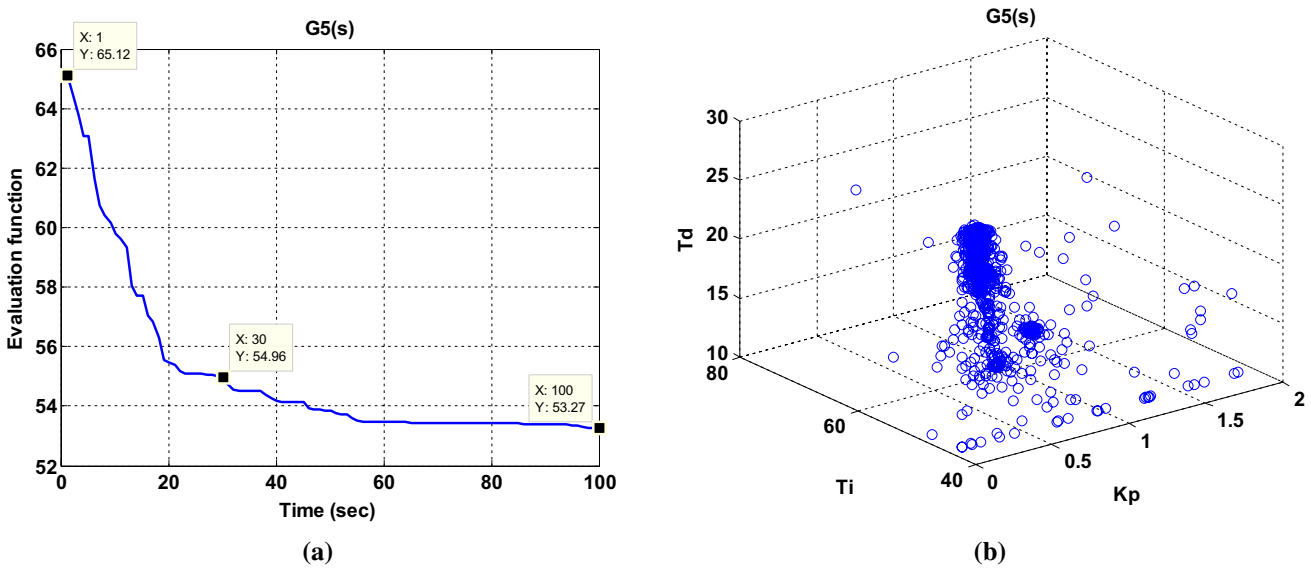

Fig. 12 **a** Evaluation function variation and **b** 3D concentration of the roots of "$G_5(s)$ process"

So, the system is stable if:

$$\begin{cases} A_1 < 0 \\ \text{and} \\ A_2 < 0 \end{cases} \Rightarrow \begin{cases} -\frac{5}{2}\left[K_p - \sqrt{(K_p)^2 - \frac{4}{5}K_iK_p}\right] < 0 \\ \text{and} \\ -\frac{5}{2}\left[K_p + \sqrt{(K_p)^2 - \frac{4}{5}K_iK_p}\right] < 0 \end{cases} \tag{33}$$

According to Eq. (33), the system is stable if:

$$K_i > 0 \text{ and } K_p > 0. \tag{34}$$

6.2 IP Speed Controller Tuned by RTO

An IP controller is implemented to improve the dynamic response and to reduce or eliminate the steady-state error.

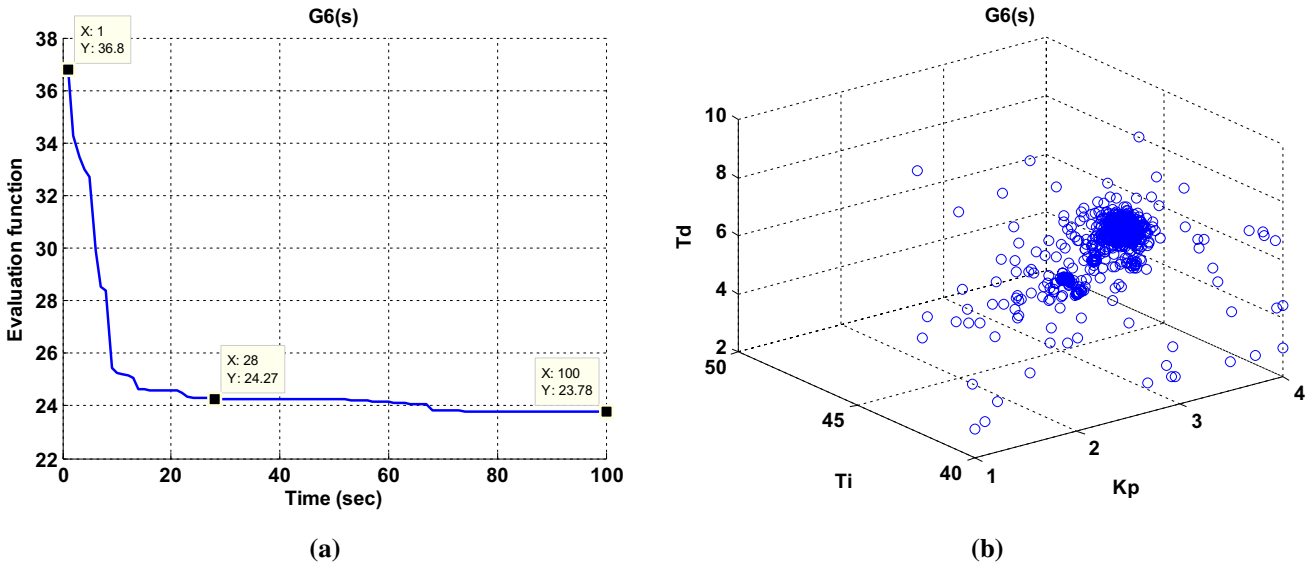

(a) **(b)**

Fig. 13 **a** Evaluation function variation and **b** 3D concentration of the roots of "$G_6(s)$ process"

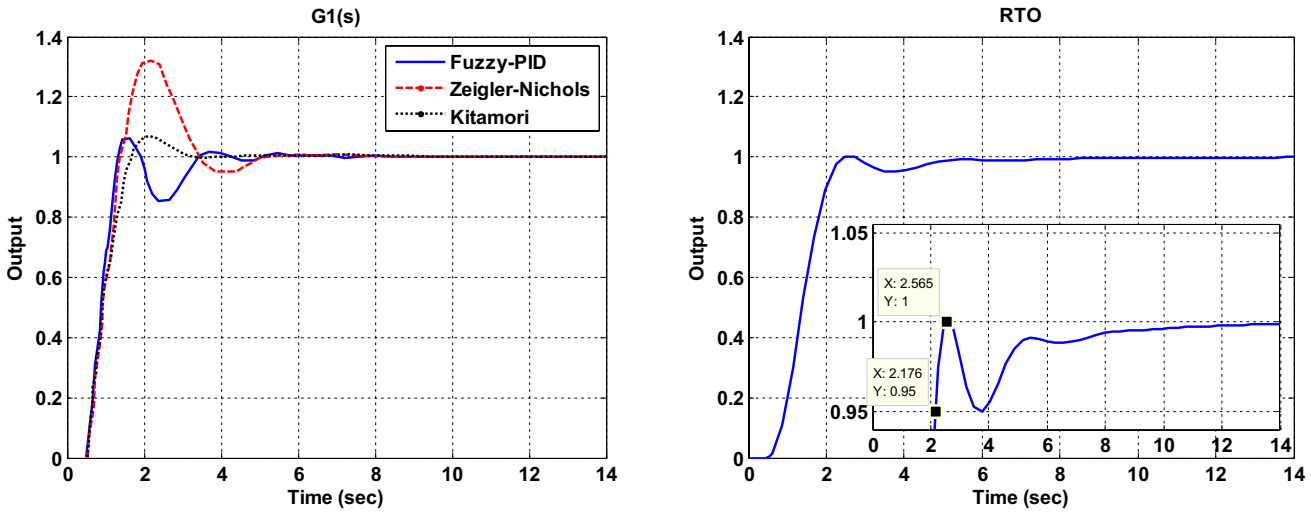

(a) [17] **(b)**

Fig. 14 Comparison of step response of the controlled "$G_1(s)$ process": **a** other methods and **b** RTO

To characterize the performance of the IP controlled system, performance of the transient response indices, such as settling time (T_s), overshoot (O_{sh}), integral absolute error (IAE), integral square error (ISE) and integral time absolute error (ITAE), must be evaluated.

Complete DTC diagram of DFIM with IP controller tuned by the RTO is presented in Fig. 6. Parameters of the DFIM are given in the Appendix. The problem here is how to tune the gains of the IP controller using the proposed system shown in Fig. 6.

After selecting an initial population, RTO is used to select the optimum parameters K_i and K_p of the IP controller by minimizing the objective function *Obj* according to Eq. (23).

In this work, each gain of K_i and K_p is coded by a number of roots that can be determined by experiment to obtain good results. Therefore, only one root (2 dimensions) represents the optimum solution values of the parameters K_i and K_p.

A flow chart of the proposed algorithm applied to an IP controller in DTC of DFIM is shown in Fig. 7. According to this, the proposed method starts with an initial random

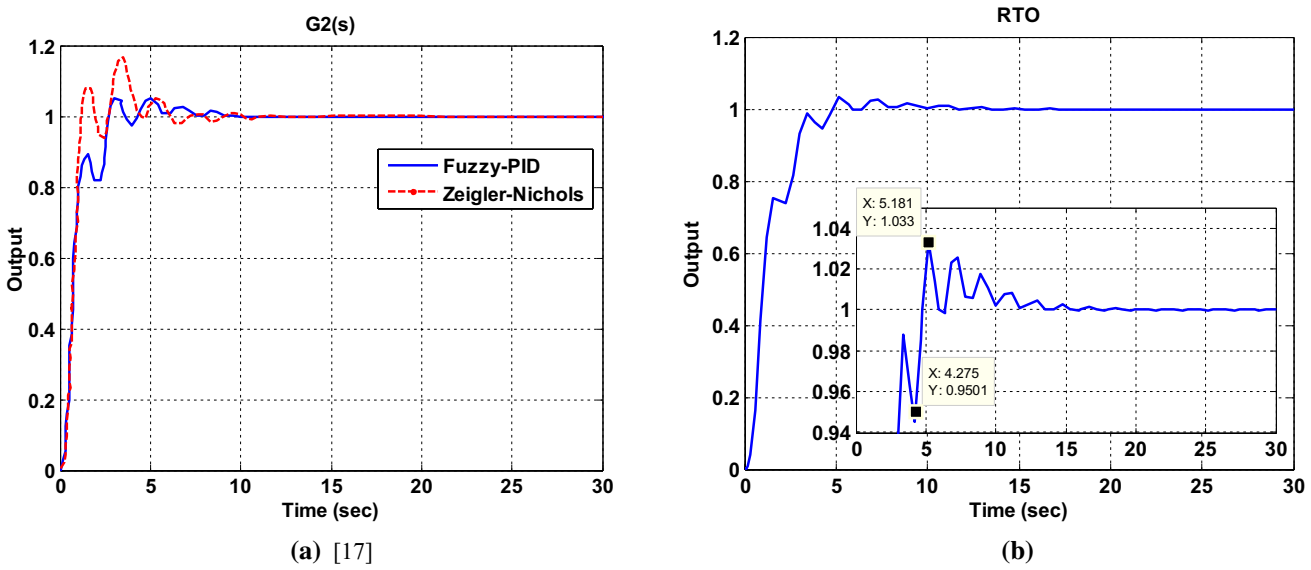

(a) [17] **(b)**

Fig. 15 Comparison of steps response of the controlled "$G_2(s)$ process": **a** other methods and **b** RTO

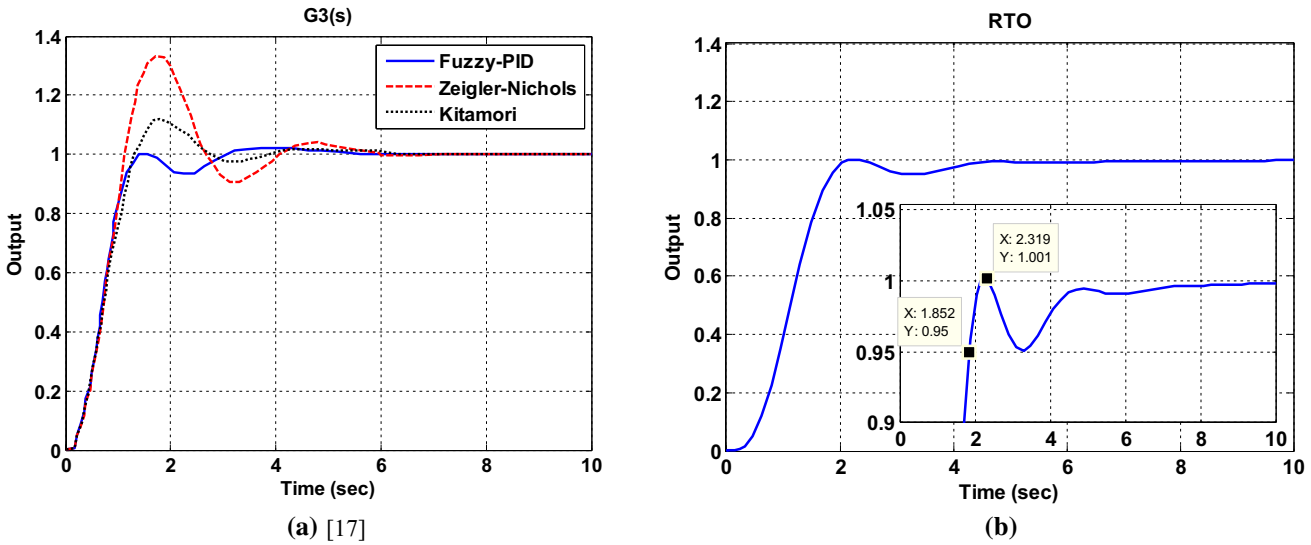

(a) [17] **(b)**

Fig. 16 Comparison of steps response of the controlled "$G_3(s)$ process": **a** other methods and **b** RTO

population for 2 dimensions (2 gains: K_i and K_p). After that, DTC-DFIM model runs to evaluate the objective function according to Eq. (23) of each individual of population. Each population (iteration) has one single minimum objective function where the best values of K_i and K_p are saved according to their minimum objective function. Operation of the optimized algorithm stops when it reaches the maximum iteration count which is the best value of minimum objective functions of all iterations.

7 Simulation Results

To verify the feasibility and efficiency of the proposed approach, two case studies are presented and implemented in MATLAB/Simulink. The first case is applied to 6 standard processes of different order controlled by a PID controller. The second case is the application of an IP controller to DTC of a DFIM.

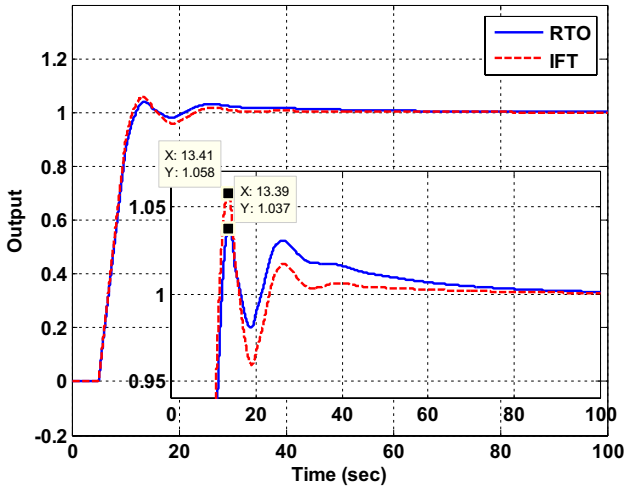

Fig. 17 Comparison of steps response of the controlled "$G_4(s)$ process" between RTO and IFT method

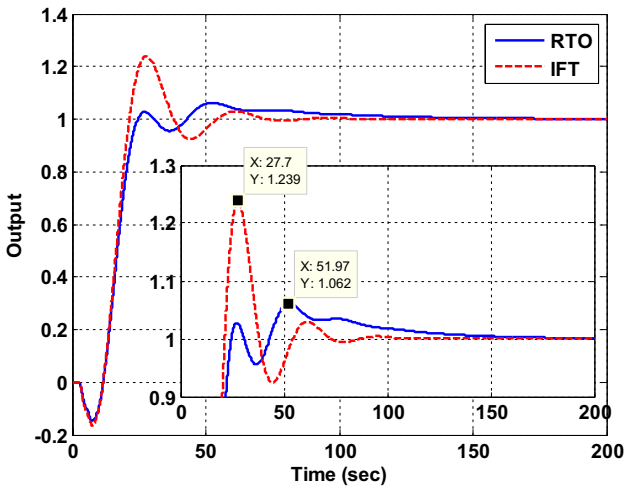

Fig. 19 Comparison of steps response of the controlled "$G_6(s)$ process" between RTO and IFT method

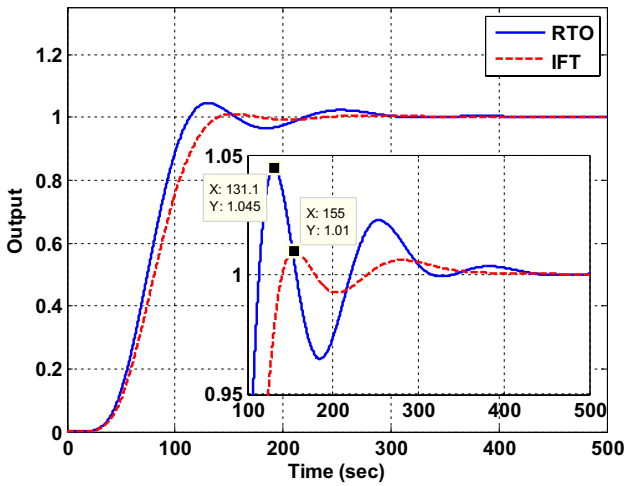

Fig. 18 Comparison of steps response of the controlled "$G_5(s)$ process" between RTO and IFT method

Parameters of the system used in simulation studies are presented in Table 3.

7.1 RTO Applied to PID Controller

In this section, the RTO was tested using objective function in Eq. (23) and compared with different methods as below:

- Ziegler–Nichols, Kitamori's and Fuzzy PID Controller for $G_1(s)$, $G_2(s)$ and $G_3(s)$ processes.
- Iterative Feedback Tuning for $G_4(s)$, $G_5(s)$ and $G_6(s)$ processes.

Evaluation function variation and the 3D concentration of the roots (candidate solutions) of $G_1(s)$, $G_2(s)$, $G_3(s)$, $G_4(s)$, $G_5(s)$ and $G_6(s)$ processes, respectively, are illustrated in Figs. 8, 9, 10, 11, 12 and 13. It is noted that the proposed approach has fast convergence towards an optimal solution in all types of processes as shown in Figs. 8a, 9a, 10a, 11a, 12a and 13a. Time responses of processes $G_1(s)$, $G_2(s)$, $G_3(s)$, $G_4(s)$, $G_5(s)$ and $G_6(s)$ with PID controller tuned using other methods and for PID controller tuned by the RTO method are plotted in Figs. 14, 15, 16, 17, 18 and 19, respectively. The optimum values of these methods and their performance compared to RTO are summarized in Tables 4 and 5.

As shown in Table 4, it is noticed that the performance of the controller tuned by the proposed approach is indeed impressive with smaller settling time and the most reduced maximum overshoot of $G_1(s)$, $G_2(s)$ and $G_3(s)$ processes. Especially for the processes $G_1(s)$ and $G_3(s)$, the value of the maximum overshoot is very small.

As seen in Table 5, the numerical results show that RTO has the smaller settling time in case of the processes $G_4(s)$ and $G_5(s)$. In addition, the proposed algorithm gives a reduced maximum overshoot in case of the processes $G_4(s)$ and $G_6(s)$.

In Tables 4 and 5:

T_s is 5 percent settling time and O_{Sh} is the percent maximum overshoot.

7.2 RTO Applied to IP Controller in DTC of DFIM

In this section, RTO is tested and compared with different values of K_i and K_p obtained by using several values of damping factor and natural frequency according to Eq. (27).

Table 4 Optimum values of RTO compared with Ziegler–Nichols, Kitamori's and Fuzzy-PID

Process	Parameters and performance	Ziegler–Nichols PID controller [17]	Kitamori's* PID controller [17]	Fuzzy PID controller [17]	PID Tuned by RTO
$G_1(s)$	K_p	2.808	2.212	/	2.1053
	T_i	1.64	2.039	/	3.2110
	T_d	0.41	0.519	/	0.5084
	T_s (s)	4.16	6.8	3.09	**2.176**
	O_{sh} (%)	32	2.37	6.0	**0**
$G_2(s)$	K_p	2.19	-	/	1.7555
	T_i	1.03	-	/	2.3041
	T_d	0.258	-	/	0.4347
	T_s (s)	5.45	-	5.01	**4.275**
	O_{sh} (%)	17	-	6.1	**3.3**
$G_3(s)$	K_p	3.072	2.357	/	2.2164
	T_i	1.352	1.649	/	2.7309
	T_d	0.338	0.414	/	0.4446
	T_s (s)	3.722	2.3	2.632	**1.852**
	O_{sh} (%)	32.8	10.9	1.9	**0.1**

The PID controller parameters of the Kitamori's controller are not available for the process $G_2(s)$ because it has a small damping ratio, 0.282 [17]

Table 5 Optimum values of RTO compared with IFT

Process	Parameters and performance	IFT- PID controller [18]	PID Tuned by RTO
$G_4(s)$	K_p	3.6717	3.5029
	T_i	27.7222	25.1120
	T_d	2.1056	2.1778
	T_s (s)	14.08	**11.13**
	O_{sh} (%)	5.8	**3.7**
$G_5(s)$	K_p	0.6641	0.8511
	T_i	53.9791	62.0167
	T_d	18.2139	21.8494
	T_s (s)	124.3537	**106.5127**
	O_{sh} (%)	**1**	4.5
$G_6(s)$	K_p	3.0279	2.6176
	T_i	46.3178	40.7818
	T_d	6.0793	8.3066
	T_s (s)	**48.21**	55.02
	O_{sh} (%)	23.9	**6.2**

Results of simulation studies on DTC-DFIM model and comparison with the proposed method are for several performance indices, such as settling time, undershoot, overshoot, integral square error (ISE) and integral absolute error (IAE), are shown in Table 6.

In this paper, robustness test against the disturbance variation for the proposed DTC-DFIM-RTO is verified. Load disturbance is suddenly applied at t = 0.6 s for a 25 Ntm load torque. This load changes to 10 N m, then to 25 N m and after that to 15 N m at t = 1.5 s, t = 2 s and 2.5 s, respectively.

Evaluation function variation is presented in Fig. 20. Variation of the two-dimensional parameters (K_i and K_p) with the generation number and their optimal values variation where the global best values are $K_i = 11.35$ and $K_p = 13.85$ is shown in Fig. 21. In Fig. 21.a, three kinds of roots appear: random roots, roots when they reach the

Table 6 Performance indices of the proposed and pole placement method

Method performance	Pole placement method (Eq. 27)					RTO
	Case 1	Case 2	Case 3	Case 4	Case 5	
	$\xi = 0.7$ $\omega_n = 13$	$\xi = 0.6$ $\omega_n = 13$	$\xi = 0.55$ $\omega_n = 13$	$\xi = 0.6$ $\omega_n = 11$	$\xi = 0.6$ $\omega_n = 9$	
K_i	9.2857	10.8333	11.8182	9.1667	7.5000	11.35
K_p	3.6400	3.120	2.8600	2.6400	2.1600	13.85
T_s (s)	0.2545	0.2008	0.1761	0.2379	0.2913	**0.1561**
U_{sh} (%)	3.3121	3.6306	3.8854	4.2038	5.0955	**0.7006**
O_{sh} (%)	1.9669	2.1839	2.4743	2.5467	3.1662	**0.6005**
ISE	1687	1554	1513	1838	2254	**1505**
IAE	18.99	16.9	16.45	20.39	25.63	**13.99**

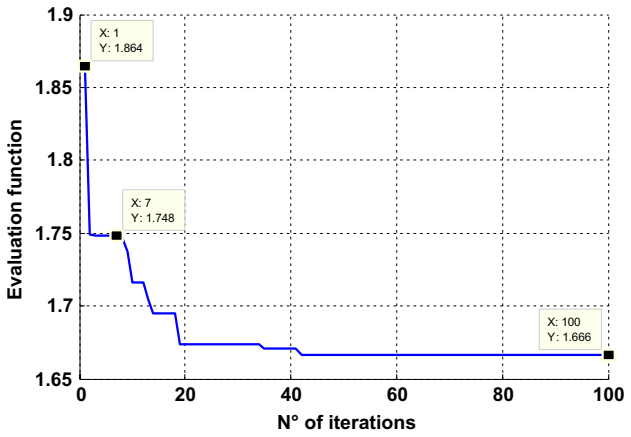

Fig. 20 Evaluation function

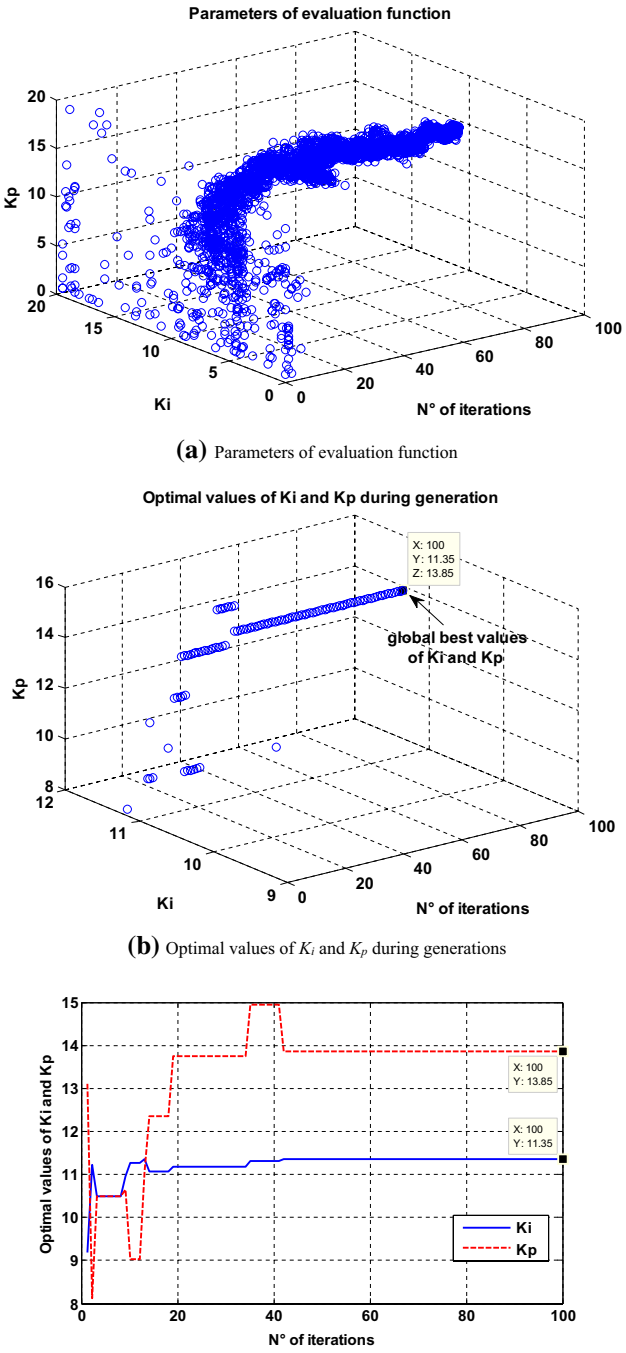

(a) Parameters of evaluation function

(b) Optimal values of K_i and K_p during generations

(c) Variation of optimal value of K_i and K_p with generations

Fig. 21 Two-dimensional variation of parameters K_i and K_p and their optimal values during

solution and the rest represent those roots that stop when they become weak compared to other roots of the same generation. Speed response of these global best values of K_i and K_p is presented in Fig. 22. Speed responses for different K_i and K_p of the pole placement method and RTO with zoom at start up and at load disturbance variation are presented in Fig. 23.

According to the obtained results from all responses of values of pole placement method as shown in Table 6 and Fig. 23, it is found that the rapidity of the response (settling time) and the stability (overshoot) are inversely related. As shown in case 3, it has smaller indices of settling time, ISE and IAE compared with the other cases but case 1 has the most reduced undershoot and overshoot.

Otherwise, the response of the proposed approach gives better performance (most reduced values of all indices) than the other cases as shown in Table 6 with 0.1561 s. settling time, 0.7006% undershoot, 0.6005% overshoot, 1505 ISE and 13.99 IAE. Stator flux trajectory in $\alpha - \beta$ axes and its 3D representation with RTO are presented in Fig. 24. Torque response of the proposed method is quick and fast dynamic response is shown in Fig. 25.

According to the simulation results, it is clear that the speed responses of the proposed and all cases of the classical method (pole placement) are affected, in transient state, at the instants of the applied load disturbance as shown in Fig. 23. Furthermore, in steady state, these responses are stabilized and remain at the reference value 157 rad/s. On the other hand, the proposed DTC-DFIM-RTO presents good stability, against the load disturbance variation with quickly rejection of this disturbance, and gives better performance in terms of fastest response, most reduced undershoot and overshoot and smallest performance indexes in time domain, ISE and IAE, compared to the classical method.

7.3 Robustness Test of Parameter Sensitivity for the Proposed DTC-DFIM-RTO

The DTC operation is basically based on the estimated stator flux using Eqs. (7) and (8). The value of this stator flux

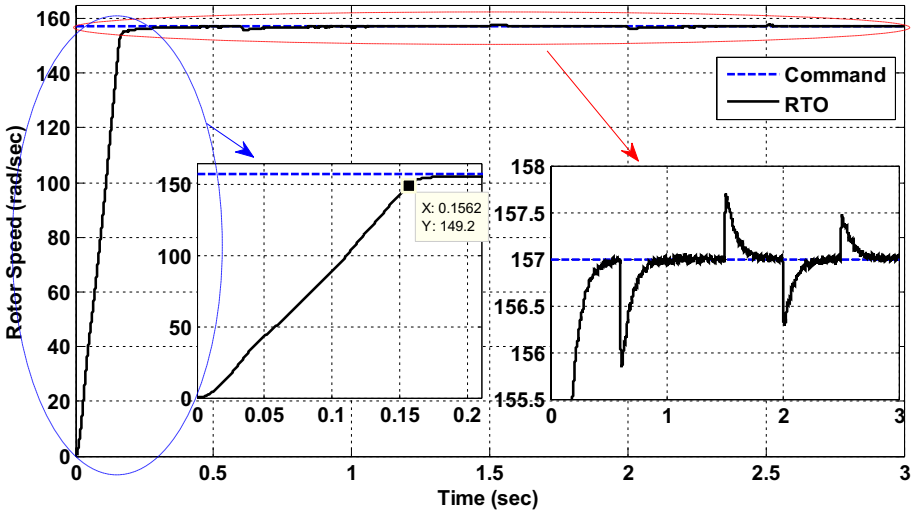

Fig. 22 Speed response for the global best values of K_i and K_p

is mostly related to the stator resistance value (R_s) which changes as a temperature function. To validate the influence of DFIM parameter variation on the performance of the proposed DTC-DFIM-RTO, sensitivity of the stator resistance parameter is tested for + 100% of its rated value.

Speed response, stator flux trajectory in $\alpha - \beta$ axes and its 3D representation and torque response with the proposed method under stator resistance variation are presented in Figs. 26, 27 and 28, respectively. After these figures, it is shown, that the proposed method is almost has the same performance in case of the rated parameter, where the speed of DFIM tracks its reference value with good control as shown in Fig. 26, however, this figure shows a little affect on the speed response in transient state. In Fig. 27, the stator flux remains stable around its desired trajectory. Torque response, as depicted in Fig. 28, shows approximately the same performance compared to the results of the rated value of stator resistance. After the results of this test, it is clear that the proposed method is robust against the variation of stator resistance.

Finally, the values of K_i and K_p tuned by the RTO show better improvement than the values obtained by the classical method (pole placement method) as fast response, reduced undershoot and overshoot appeared and quickly disappeared during load variation with small integral square error and integral absolute error. Consequently, the proposed method has a small area of error between the command and the output of the speed under closed-loop as shown in Table 6 and Fig. 23.

8 Conclusions

A rooted tree optimization (RTO) algorithm is presented and implemented to tune the gains of an IP controller used in direct torque control of a doubly fed induction machine in motor mode. The proposed method is first applied to a PID controller for different processes to show its effectiveness in minimizing a multi-objective function in control system. The proposed approach applied to tune the parameters of a PID controller gives better performance response compared to some classical methods as Ziegler–Nichols, Kitamori's, Fuzzy-PID and Iterative Feedback Tuning. In addition, the results in this case show an improvement in settling time with reduced maximum undershoot and overshoot. In the case of an IP controller used in DTC of DFIM, the results show better performance in speed response compared with different values of K_i and K_p obtained by using the classical method based on pole placement method. Therefore, RTO gives better improvement in control system than the other common tuning methods. Furthermore, to validate the influence of the DFIM parameter variation on the performance of the proposed DTC-DFIM-RTO, sensitivity of the stator resistance parameter is tested for + 100% of its rated value. Simulation results show that the proposed method is robust against parameter variation and able to reject its influence.

According to the simulation results based at the new proposed tuning method using RTO, the main improvements presented in this paper are:

- In case of PID controller:
- Fast response of the outputs of various processes in transient state.
- Reduction of the maximum undershoot and overshoot of the outputs response in transient and steady state.

In case of IP controller:

- Fast response of the speed of DFIM for DTC in transient state.
- Reduction of the maximum undershoot and overshoot of the speed response in transient and steady state.

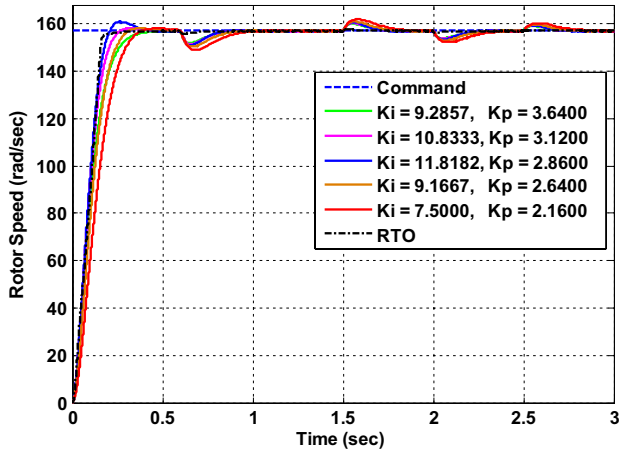

(a)

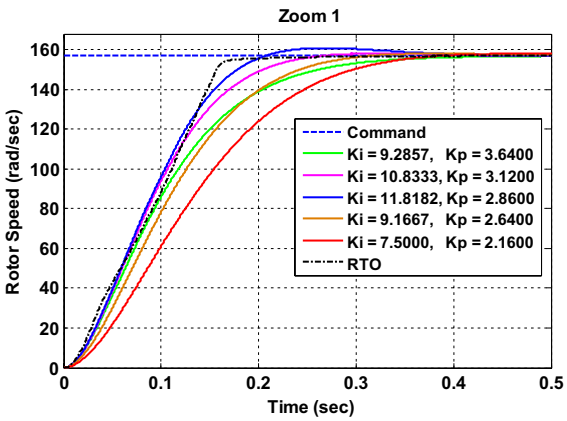

(b)

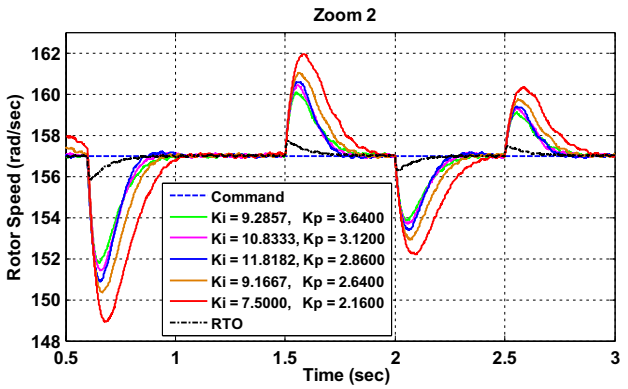

(c)

Fig. 23 **a** Speed response for different K_i and K_p compared to RTO, with a zoom **b** in start up and **c** at load disturbance variation

- Reduction of values of integral square error (ISE) and integral absolute error (IAE) for the speed response. Therefore, a small area of error between the command and the output of the speed.

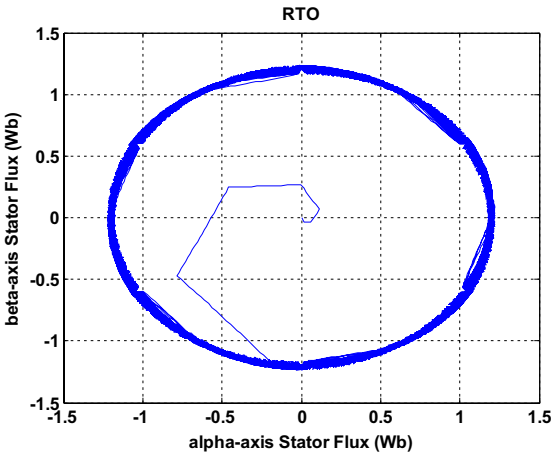

(a)

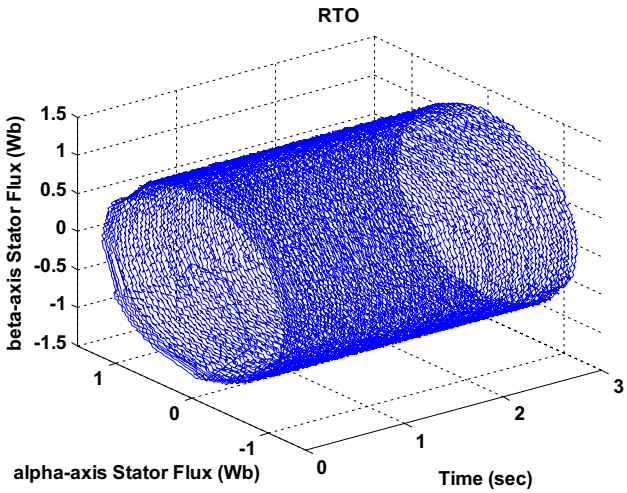

(b)

Fig. 24 **a** Stator flux trajectories of α–β axes and **b** its 3D representation with RTO

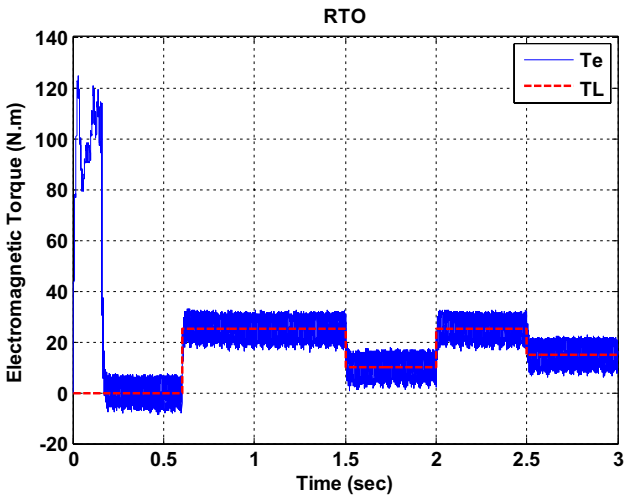

Fig. 25 Torque response with the proposed RTO

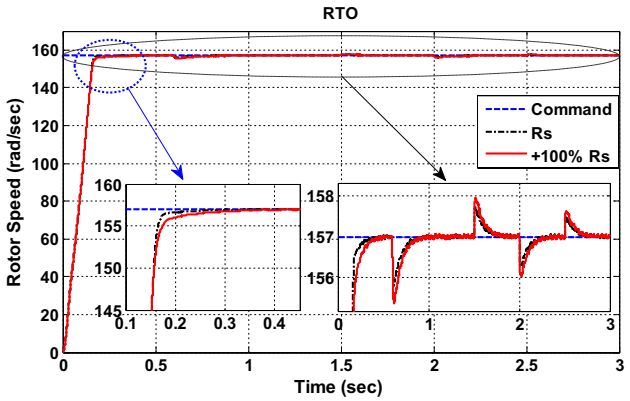

Fig. 26 Speed response for the global best values of K_i and K_p under stator resistance variation

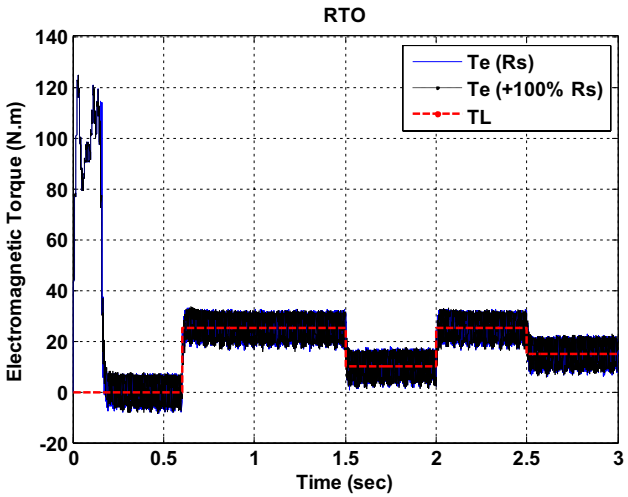

Fig. 28 Torque response with the proposed RTO under stator resistance variation

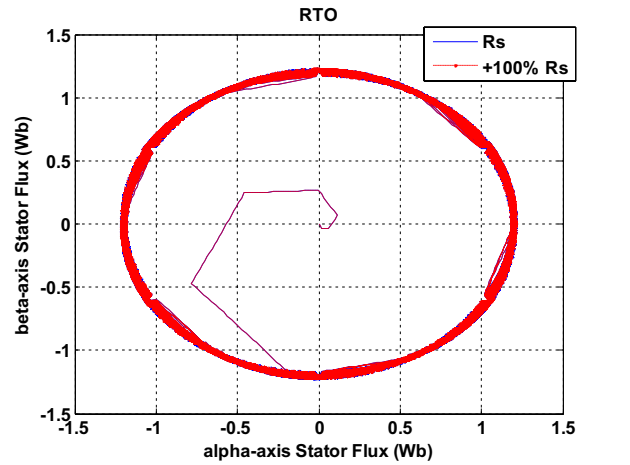

Fig. 27 **a** Stator flux trajectories of α–β axes and **b** its 3D representation with RTO under stator resistance variation

Appendix 1: DFIM Parameters

Rated values
4 kW, 220/380 V, 1440 rpm
Rated parameters
$R_s = 1.2\ \Omega$
$R_r = 1.8\ \Omega$
$L_s = 0.1554$ H
$L_r = 0.\ 1568$ H
$M = 0.15$ H
$P = 2$
Mechanical constants
$J = 0.2$ kg m^2
$f = 0.0$ N m s/rad

Appendix 2: Nomenclature

DFIM

$V_{s\alpha}$, $V_{s\beta}$	Stator α, β frame voltages
$V_{r\alpha}$, $V_{r\beta}$	Rotor α, β frame voltages
$i_{s\alpha}$, $i_{s\beta}$	Stator α, β frame currents
$i_{r\alpha}$, $i_{r\beta}$	Rotor α, β frame currents
$\varphi_{s\alpha}$, $\varphi_{s\beta}$	Stator α, β frame fluxes
$\varphi_{r\alpha}$, $\varphi_{r\beta}$	Rotor α, β frame fluxes
$R_{s\alpha}$, R_r	Stator and rotor resistances
$L_{s\alpha}$, L_r	Stator and rotor inductances
M	Mutual inductance
σ	Leakage factor
T_s, T_r	Stator and rotor time-constant
Ω_r	Rotor speed
T_e	Electromagnetic torque

T_L	Load torque
J	Moment of inertia
f	Friction coefficient
p	number of pole pairs
ω_r	Rotor angular speed

RTO

x^{new}	New candidate
x^{best}	Best solution
k	Candidate number
iter	Iteration
N	Population scale
upper	Upper limit
randn	Normal random number between [− 1, 1]
rand	Number between [0, 1]
R_n	Rate of the random root
R_r	Rate of the random root
R_c	Rate of the continuous root

Acronyms

DFIM	*Doubly Fed Induction Machine/Motor*
DTC	*Direct Torque Control*
FOC	*Field Oriented Control*
IP	*Integral Proportional*
RTO	*Rooted Tree Optimization*
VC	*Vector Control*
2D/ 3D	*Two / Three-dimensional*

Acknowledgements The authors would like to acknowledge support from Directorate General for Scientific Research and Technological Development (DGRSDT), Ministry of Higher Education and Scientific Research—Algeria.

References

1. Yu K, Tang P (2018) Novel Equivalent Circuit Model and Theoretical Analysis of Doubly Fed Machine. IEEE Trans Energy Convers 34:1073–1081
2. El Ouanjli N, Derouich A, El Ghzizal A, Chebabhi A, Taoussi M (2017) A comparative study between FOC and DTC control of the Doubly Fed Induction Motor (DFIM). In: International conference on electrical engineering and information technology. IEEE, pp 1–6
3. BonnetFrancois F, Vidal P-E, Pietrzak-David M (2007) Dual direct torque control of doubly fed induction machine. IEEE Trans Indu Electro 54(5):2482–2490
4. Babouri R, Aouzellag D, Ghedamsi K (2013) Introduction of doubly fed induction machine in an electric vehicle. Ener Procedia 36:1076–1084
5. Jain JK, Ghosh S, Maity S, Dworak P (2017) PI controller design for indirect vector controlled induction motor: a decoupling approach. ISA Trans 70:378–388
6. Takahashi I, Ohmori Y (1989) High-performance direct torque control of an induction motor. IEEE Trans Ind Appl 25(2):257–264
7. Zemmit A, Messalti S, Harrag A (2017) A new improved DTC of doubly fed induction machine using GA-based PI controller. Ain Shams Eng J 9:1877–1885
8. Kumsuwan Y, Premrudeepreechacharn S, Toliyat HA (2008) Modified direct torque control method for induction motor drives based on amplitude and angle control of stator flux. Electric Power Syst Res 78(10):1712–1718
9. Gadoue SM, Giaouris D, Finch J (2009) Artificial intelligence-based speed control of DTC induction motor drives—a comparative study. Electric Power Syst Res 79(1):210–219
10. Sarasola I, Poza J, Rodriguez MA, Abad G (2011) Direct torque control design and experimental evaluation for the brushless doubly fed machine. Energy Convers Manag 52(2):1226–1234
11. Carmeli M, Mauri M (2011) Direct torque control as variable structure control: Existence conditions verification and analysis. Electric Power Syst Res 81(6):1188–1196
12. Abdelli R, Rekioua D, Rekioua T (2011) Performances improvements and torque ripple minimization for VSI fed induction machine with direct control torque. ISA Trans 50(2):213–219
13. Lazim MT, Al-khishali MJ, Al-Shawi AI (2011) Space vector modulation direct torque speed control of induction motor. Proc Comput Sci 5:505–512
14. Orlowska-Kowalska T, Tarchala G, Dybkowski M (2014) Sliding-mode direct torque control and sliding-mode observer with a magnetizing reactance estimator for the field-weakening of the induction motor drive. Math Comput Simul 98:31–45
15. Ziegler JG, Nichols NB (1942) Optimum settings for automatic controllers. Trans ASME 64(11):759–765
16. Kitamori T (1979) A method of control system design based upon partial knowledge about controlled processes. Trans Soc Inst Control Eng 15(4):549–555
17. Zhao Z-Y, Tomizuka M, Isaka S (1993) Fuzzy gain scheduling of PID controllers. IEEE Trans Syst Man Cyber 23(5):1392–1398
18. Lequin O, Gevers M, Mossberg M, Bosmans E, Triest L (2003) Iterative feedback tuning of PID parameters: comparison with classical tuning rules. Control Eng Pract 11(9):1023–1033
19. Chaouch S, Abdou L, Alaoui LC, Drid S (2016) Optimized torque control via backstepping using genetic algorithm of induction motor. Automatika 57(2):379–386
20. Mesloub H, Benchouia M, Goléa A, Goléa N, Benbouzid M (2017) A comparative experimental study of direct torque control based on adaptive fuzzy logic controller and particle swarm optimization algorithms of a permanent magnet synchronous motor. Int J Adv Manuf Technol 90(1–4):59–72
21. Hannan M, Ali JA, Mohamed A, Hussain A (2017) Optimization techniques to enhance the performance of induction motor drives: a review. Renew Sustain Energy Rev 81:1611–1626
22. Kumar DS, Sree RP (2016) Tuning of IMC based PID controllers for integrating systems with time delay. ISA Trans 63:242–255
23. Juang Y-T, Chang Y-T, Huang C-P (2008) Design of fuzzy PID controllers using modified triangular membership functions. Info Sci 178(5):1325–1333
24. Padula F, Visioli A (2011) Tuning rules for optimal PID and fractional-order PID controllers. J Proc Control 21(1):69–81
25. Harrag A, Messalti S (2015) Variable step size modified P&O MPPT algorithm using GA-based hybrid offline/online PID controller. Renew Sustain Energy Rev 49:1247–1260

26. Srivastava S, Pandit V (2016) A PI/PID controller for time delay systems with desired closed loop time response and guaranteed gain and phase margins. J Proc Control 37:70–77
27. Anil C, Sree RP (2015) Tuning of PID controllers for integrating systems using direct synthesis method. ISA Trans 57:211–219
28. Moharam A, El-Hosseini MA, Ali HA (2016) Design of optimal PID controller using hybrid differential evolution and particle swarm optimization with an aging leader and challengers. Appl Soft Comput 38:727–737
29. Liem DT, Truong DQ, Ahn KK (2015) A torque estimator using online tuning grey fuzzy PID for applications to torque-sensorless control of DC motors. Mechatro 26:45–63
30. Ye Y, Yin C-B, Gong Y, Zhou J-J (2017) Position control of nonlinear hydraulic system using an improved PSO based PID controller. Mech Syst Sign Proc 83:241–259
31. Lu K, Zhou W, Zeng G, Du W (2018) Design of PID controller based on a self-adaptive state-space predictive functional control using extremal optimization method. J Frankl Inst 355(5):2197–2220
32. Labbi Y, Attous DB, Gabbar HA, Mahdad B, Zidan A (2016) A new rooted tree optimization algorithm for economic dispatch with valve-point effect. Int Electr Power Energy Syst 79:298–311
33. Sannigrahi S, Ghatak SR, Acharjee P (2019) Fuzzy logic–based rooted tree optimization algorithm for strategic incorporation of DG and DSTATCOM. Int Trans Electr Ener Syst 29(8):e12031
34. Wadood A, Gholami Farkoush S, Khurshaid T, Kim C-H, Yu J, Geem ZW et al (2018) An optimized protection coordination scheme for the optimal coordination of overcurrent relays using a nature-inspired root tree algorithm. Appl Sci 8(9):1664
35. Sannigrahi S, Ghatak SR, Acharjee P (2018) Optimal planning of distribution network with DSTATCOM and WTDG using RTO technique. In: International power electronics, drives, and energy systems (PEDES) conference. IEEE, pp 1–6
36. Benamor A, Benchouia M, Srairi K, Benbouzid M (2019) A new rooted tree optimization algorithm for indirect power control of wind turbine based on a doubly-fed induction generator. ISA Trans 88:296–306
37. Benamor A, Benchouia M, Srairi K, Benbouzid M (2019) A novel rooted tree optimization apply in the high order sliding mode control using super-twisting algorithm based on DTC scheme for DFIG. Int J Electr Power Energy Syst 108:293–302
38. Cui Y, Geng Z, Zhu Q, Han Y (2017) Multi-objective optimization methods and application in energy saving. Energy 125:681–704
39. El-Samahy AA, Shamseldin MA (2018) Brushless DC motor tracking control using self-tuning fuzzy PID control and model reference adaptive control. Ain Shams Eng J 9(3):341–352
40. Ben Jabeur C, Seddik H (2020) Design of a PID optimized neural networks and PD fuzzy logic controllers for a two-wheeled mobile robot. Asian J Control 23:23–41
41. Kumar NS, Gokulakrishnan J (2011) Impact of FACTS controllers on the stability of power systems connected with doubly fed induction generators. Int J Electr Power Ene Syst 33(5):1172–1184
42. Maciejewski P, Iwanski G (2017) Direct torque control for autonomous doubly fed induction machine based DC generator. In: 2017 twelfth international conference on ecological vehicles and renewable energies (EVER). IEEE, pp 1–6
43. Takahashi I, Noguchi T (1986) A new quick-response and high-efficiency control strategy of an induction motor. IEEE Trans Ind Appl 5:820–827
44. Boudana D, Nezli L, Tlemçani A, Mahmoudi M, Tadjine M (2012) Robust DTC based on adaptive fuzzy control of double star synchronous machine drive with fixed switching frequency. J Electr Eng 63(3):133–143
45. Do TD, Choi HH, Jung J-W (2015) Nonlinear optimal DTC design and stability analysis for interior permanent magnet synchronous motor drives. IEEE/ASME Trans Mechatron 20(6):2716–2725
46. Verma A, Singh B, Yadav D (2014) Investigation of ANN tuned PI speed controller of a modified DTC induction motor drive. In: 2014 IEEE international conference on power electronics, drives and energy systems (PEDES). IEEE, pp 1–6
47. Sudheer H, Kodad S, Sarvesh B (2017) Improvements in direct torque control of induction motor for wide range of speed operation using fuzzy logic. J Electri Syst Inf Technol 5:813–828
48. Soufi Y, Bahi T, Lekhchine S, Dib D (2013) Performance analysis of DFIM fed by matrix converter and multi level inverter. Energy Conv Manag 72:187–193
49. Sreekumar T, Jiji K (2012) Comparison of proportional-integral (PI) and integral-proportional (IP) controllers for speed control in vector controlled induction motor drive. In: 2012 2nd international conference on power, control and embedded systems. IEEE, pp 1–6
50. Hwang C, Cheng Y-C (2006) A numerical algorithm for stability testing of fractional delay systems. Automatica 42(5):825–831